SUMIC: A Simple Ultrafast Multicolor Immunolabelling and Clearing Approach for Whole-Organ and Large Tissue 3D Imaging

Lincoln Biswas[1,#], Junyu Chen[1,5,#], Jessica De Angelis[1], Alexandros Chatzis[1], Jagdeep Nanchahal[2], Michael L. Dustin[2], Saravana K. Ramasamy[3,4], Anjali P. Kusumbe[1,*]

[1]Tissue and Tumor Microenvironments Group, University of Oxford, Kennedy Institute of Rheumatology, NDORMS, Oxford, OX3 7FY, UK

[2]University of Oxford, Kennedy Institute of Rheumatology, Oxford, OX3 7FY, UK

[3]Institute of Clinical Sciences, Imperial College London, London W12 0NN, UK

[4]MRC London Institute of Medical Sciences, Imperial College London, London W12 0NN, UK

[5]Department of Prosthodontics, State Key Laboratory of Oral Diseases, West China Hospital of Stomatology, Sichuan University, Chengdu 610041, China

*Author for correspondence:
Anjali P. Kusumbe
Kennedy Institute of Rheumatology
University of Oxford
Roosevelt Drive
Headington
Oxford OX3 7FY, UK
anjali.kusumbe@kennedy.ox.ac.uk
Phone: +44 01865 612 668

[#] These authors contributed equally

Keywords: 3D imaging, blood vessels, lymphatic vessels, tissue clearing, light sheet

Abstract

High-resolution whole-organ imaging of cleared tissues captures cellular and molecular insights within the intact tissue and tumour microenvironments. However, current immunolabelling and clearing methods are complicated and time-consuming; extending to several weeks. Here, we developed **S**imple **U**ltrafast **M**ulticolor **I**mmunolabelling and **C**learing or **SUMIC**, a method that enables multicolor immunolabelling and clearing of whole murine organs and human tissues within 2 to 2.5 days. Moreover, SUMIC is simple, robust, non-hazardous and versatile comprising antigen retrieval, permeabilization, collagenase-based digestion, immunolabelling, dehydration, and clearing. SUMIC permits quantitative and single-cell resolution analysis and detection of rare cells in whole organs, for example, round αSMA positive cells in the thymus. Upon volumetric imaging, SUMIC-processed samples retain normal tissue architecture and can be used for paraffin-embedding and histology. We employed the SUMIC method for whole-organ mapping of lymphatic vessels across different ages and organs. This analysis revealed the expansion of lymphatic vessels in endocrine tissues but not in any other organs with aging. Hence, SUMIC will accelerate discoveries compared to other whole organ imaging pipelines.

Introduction

Advanced 3D imaging approaches provide critical insights into the fundamentals of highly complex biological processes during organ development, regeneration, repair and pathology (*1-7*). To advance our understanding of such processes, it is vital to generate accurate cellular, and molecular cartography of healthy, aged, diseased and malignant tissues is vital (*8-11*). The 3D analysis of intact biological specimens reveals essential structural and spatial information necessary for the understanding of the crosstalk among various cell types in the tissue context (*9, 12-16*). Moreover, deciphering the organization of the nervous and vascular systems relies on a whole organ approach (*12, 17-20*). This treasure trove of information comes at the expense of detailed and complicated requirements for time-consuming sample processing, imaging, data storage, analysis and interpretation, which can be met by a range of recent technical developments.

The recent development of tissue clearing, light sheet microscopy and large dataset analysis has made it possible to image large volumes at single-cell resolution (*13, 21-23*). However, current protocols for immunostaining and whole organ clearing are often time-consuming, elaborate, expensive, and organ-specific (*24-32*). The time-consuming nature of the whole organ and large tissue imaging is the main obstacle to overcome before efficiently applying this crucial technique to understand biological complexity and interrogating cellular interactions within tissues and organs. Other disadvantages include the requirement for transgenic mice that express fluorescent

reporters and the use of toxic or corrosive chemicals that might be detrimental either to the microscope or researcher's well-being (*11, 33-35*).

Therefore, it is essential to develop a rapid method for whole organ and large tissue multicolor immunostaining coupled with a technique applicable for diverse tissues while preserving endogenous fluorescence. Here we devised a new robust and straightforward method- **S**imple **U**ltrafast **M**ulticolor **I**mmunolabelling and **C**learing or SUMIC which permits immunostaining and clearing of multiple whole organs and large tissues in a record time of 2.5 days, and also overcomes other limitations of current methods.

Results

SUMIC: an ultrafast immunostaining and clearing method for murine organs and human tissues

In SUMIC we set out to develop a platform that is able to attain a multicolor immunolabelling together with excellent cellular morphology, tissue architecture and transparency across multiple murine organs and human tissues. Each of the 10 steps were optimized to enable completion in the shortest possible time (Fig. 1). First, we combined paraformaldehyde and glutaraldehyde for rapid fixation (Step 1). Samples were bleached with hydrogen peroxide in methanol to eliminate heme and other persistent chromophores (Step 2). Urea facilitated antigen retrieval, and Triton X-100 increased the penetration depth of antibodies into tissues while maintaining tissue architecture (Step 3). Collagenase-digestion of the extracellular matrix significantly improved the penetration rate of the antibodies while keeping the structure of the tissues intact (Step 4). To obtain good staining, only antibodies labelled with small,

4

bright fluorochromes with high stability and good tissue penetrance, such as Alexa Fluor dyes, were used (Step 5). Triton X 100, a mild detergent was included for blocking, staining and washing the organs during this step. Incubations with antibodies and their washings were performed at 37°C to reduce the time requirement further. Dehydration is a crucial step that precedes tissue clearing and RI matching (Step 6). Dehydration using isopropanol preserved all fluorochromes and resulted in less tissue shrinkage compared to ethanol. Ethyl cinnamate (ethyl 3-phenyl-2-propenoate; ECi) is non-toxic and has been utilized for tissue clearing (*11*). Poly(ethylene glycol) methyl ether methacrylate (PEGM) has also been used as a component of tissue clearing solutions (*26*). For SUMIC ECi (80%) and PEGM (20%) were combined. This combination of ECi and PEGM cleared all the tested organs and tissues within 2 hours (Step 7). ECi was used for RI matching for imaging (Step 8). Starting from collecting the organs to image acquisition, SUMIC protocol for multicolor antibody labelling and tissue clearing required up to 2.5 days with conjugated antibodies (Fig. 1). SUMIC also includes a rendering and analysis pipeline (Step 9).

Finally, after SUMIC, the clarified tissues could be sectioned histopathology (Step 10).

We have successfully validated SUMIC across multiple murine organs, including lung, heart, kidney, liver, gut, spleen, thymus, prostate gland, seminal vesicle and endocrine glands (Fig. 2, Fig. 3, Fig. S1 and Movie 1-6). Notably, a few organs, such as liver, demonstrated a slightly brownish yellow colour even after the completion of the clearing process (Fig. 2D); however, this had minimal impact on the penetration depth of the light sheet. We selected ~40 of antibodies to test and validate SUMIC method across multiple organs and tissues. We selected antibodies for the cell and matrix molecules expressed across different organs. The cell markers defining vascular and

5

tissue microenvironments, including endothelial cells, pericytes, mesenchymal cells and immune cells, were used. Endothelial cell markers; Endomucin (Emcn), Endoglin (CD105), CD31 also known as PECAM1 and CD102 (ICAM2); α-SMA staining was used for artery quantifications, and pericytes were identified by PDGFRβ and NG2. Lymphatic vessels were analyzed by LYVE1 and Prox1. We provide full information for each of these antibodies and their working conditions (Table S1). With these cell surface markers, SUMIC enabled 3D imaging of blood vessels and associated niches across several organs and endocrine glands (Fig. 2, Fig. 3, Fig. S1 and Movie 1-6). Thus, the SUMIC method provided the flexibility of usage across multiple organs and tissues. Troubleshooting tips relevant to the SUMIC method can be found in Table S2, and the methods section of the paper. In addition to the murine organs, SUMIC permitted ultrafast immunostaining and clearing of human tissues (Fig. 4, A and B).

SUMIC preserves tissue architecture and endogenous GFP/tomato fluorescence

To determine the effect of SUMIC processing on tissue morphology, we embedded SUMIC-processed organs in paraffin and examined the samples previously imaged in 3D by conventional histology. 2D histology showed that SUMIC processed tissues remained accessible to a conventional histological analysis by haematoxylin and eosin (Fig. S2). Tissue architecture remained unaffected, and different structures, such as blood vessels, were detected in SUMIC processed tissues similar to the control tissues processed by conventional paraffin embedding (Fig. S2). Thus, SUMIC enabled rapid, deep tissue immunolabeling and clearing of intact organs while maintaining tissue architecture.

Endogenous fluorescence loss is a crucial concern for solvent-based tissue clearing medium and other steps during tissue processing. To assess the impact of SUMIC clearing on endogenous fluorescence either *Flk1 GFP* or *CDh5 Cre ERT2 X td-tomato* mice was used. Our analysis revealed that the SUMIC processed samples preserved tomato and GFP fluorescence (Fig. 4, C and D).

SUMIC permits single-cell resolution analysis in whole-organs

Light sheet microscopy was used to perform volumetric imaging and thereby produce the whole organ and tissue overviews of SUMIC-processed murine whole organs and human tissues. We next aimed at transitioning from a general overview of the complete tissue to the analysis of specific regions within the tissue at the single-cell resolution. Subsequently, computational surface rendering was applied to the regions of interest, which provides single-cell level information from three-dimensional tile scan images (Fig. 4, E and F). This analysis led to the detection of a small subset of round α-smooth muscle actin positive cells within the cortex region of the thymus in addition to the usual periarteriolar location of these cells (Fig. 4E). Such round α-SMA positive monocyte-macrophage subset has been reported in the bone marrow where these cells preserve primitive hematopoiesis (*36*). However, such a small subset of α-SMA positive monocytes-macrophages has not been reported to be present in the thymus.

SUMIC enables quantitative imaging of whole organ overviews

Next, we carried out a quantitative analysis of the lymphatic vessels in 3D by LYVE-1 and Prox1 immunostainings on whole organs and endocrine glands. The circulatory system encompasses both the blood vascular and lymphatic vascular systems. The lymphatic system regulates fluid homeostasis, waste clearance and immune

7

responses (*37, 38*). Recent studies have not only revealed age-dependent changes in blood vessels, organs and endocrine glands but also documented the correlation of these changes with the organ function (*39*). Here, we examined and compared the lymphatic vessels across different endocrine glands. Quantitative analysis of LYVE-1 and Prox1 immunostainings across endocrine glands from young and aged mice demonstrated expansion of lymphatic vessels in ovaries, testis and thyroid glands (Fig. 5, A and B). In contrast, the lymphatic vessel density remained unchanged across murine organs with age (Fig. S3).

To understand the relevance of age-related changes observed in these three murine endocrine glands, we analyzed human endocrine tissues. Healthy human testis, ovary and thyroid gland of young (<20 years) and aged (>70 years) individuals (Table S3) were tested for the *Prox1* gene by quantitative PCR (qPCR) (Fig. 5C). Likewise, murine endocrine glands, aged human ovary, testis and thyroid glands exhibited an increased *Prox1* expression (Fig. 5C). Importantly, analysis of even 4 random human samples of each of these glands showed these significant changes. These results provide evidence for the applicability of SUMIC method, which is not only rapid and robust but also holds tremendous potential in providing new insights and uncovering biological complexities.

Discussion

3D organization of functional networks, such as blood or lymphatic vessels within organs and spatial information of cells within tissues, is important to understand the biological complexity (*10, 40-43*). 3D imaging of cleared large tissues or whole organs provides this information (*12, 14, 41, 43-45*). Further, it is a valuable alternative to traditional histology or immunofluorescence of thin tissue sections, both of which lack

the crucial 3D information (*16, 45-48*). To enable rapid, simplified and high-resolution 3D imaging of whole organs and large tissue samples, we introduce and describe the SUMIC method. SUMIC enables the 3D molecular analysis of intact organs and tissue biopsies at a single-cell and subcellular resolution. A sequence of tissue alterations renders the samples susceptible to rapid and optimum immunostaining and histological staining while preserving cell and tissue integrity. Digestion of extracellular matrix by Collagenase and use of methanol increases antibody penetration. Collagenase based extracellular matrix digestion and incubation of antibodies at a higher temperature facilitate speed through rapid penetration of the antibodies. Further, these steps avoid the time-consuming delipidation steps that involve the use of highly toxic substances (*44, 49*). Further, the bleaching step reduces light scattering (*49, 50*). Hydrogen peroxide used for bleaching reduces tissue autofluorescence and is useful, particularly in tissues with high heme content, such as spleen and heart (*51*). Bleaching before the immunostaining aids in the retention of these fluorochromes which otherwise are susceptible to bleaching. Thus, SUMIC neither requires an injection of antibodies, nor it relies on transgenic mice expressing fluorescent reporters; it instead uses multicolor immunolabelling by fluorochrome-coupled antibodies.

ECi and PEGM have been used independently in various clearing methods as tissue clearing recipe components or for RI matching due to their inexpensive and flexible nature (*11, 51-53*). Here, we combined these two; ECi and PEGM, which facilitates the rapid clearing of larger tissues and organs. After clearing, images can be acquired on different imaging systems such as a laser scanning confocal microscope for single-cell and subcellular resolution or light sheet microscope for whole organ overviews. Therefore, SUMIC enables multicolor antibody-based immunolabelling, provides good

tissue transparency, and preserves cellular morphology and flexibility in microscope usage.

As a result of facilitating high speed, high resolution and flexibility in organ, tissue, fluorochrome and microscope usage, SUMIC has the tremendous potential to make tissue clearing and 3D imaging more widely accessible to a broader audience. SUMIC is a versatile technique that can be used for answering a wide variety of questions throughout the biological sciences. Thus, SUMIC adds to the tools and information needed to investigate complex biological processes that demand spatial and architectural knowledge of cells within tissues and organs.

Material and methods

Mice

Organs and endocrine glands were dissected from adult 8-15-weeks-old male and female wild-type C57BL/6J mice purchased from Jackson Laboratory and bred in-house. To examine lymphatic vessels during ageing, young mice of 8-10 weeks-old and aged mice at 56-70-week-old age were used. For the study of native fluorescence, the $Kdr^{tm2.1Jrt}$/J (54) (Stock No: 017006, Jackson Laboratory) and *ROSA26 td-Tomato* (Stock No: 007914, Jackson Laboratory) (55), were used. For genetic labelling of the vasculature, *Cdh5(PAC)-CreERT2* transgenic mice (56) were mated with *ROSA26 td-Tomato* reporters. All the animals utilized for the studies were housed in the University of Oxford. The experimental procedures on mice were performed following the UK Home Office Animal Care guidelines on the Operation of the Animals (Scientific Procedures) Act 1986 and the protocols approved by the local Animal

Welfare and Ethical Review Board and by the UK Government Home Office (Animals Scientific Procedures Group).

Tamoxifen treatment

For oral gavage of tamoxifen, tamoxifen (Sigma, T5648) was firstly dissolved in 100% ethanol and then suspended in corn oil to a final concentration of 5 mg/ml. For *Cdh5(PAC)-CreERT2; Rosa26-td-Tomato* transgenic mice, to induce Cre activity, mice were orally treated with tamoxifen at a dose of 50 mg/kg body weight for three consecutive days. Mice were sacrificed and analyzed two weeks after the last dose of tamoxifen.

Tissue collection and preparation

Freshly dissected mouse tissues were rinsed in PBS (VWR, cat. No. 437117K) and then immediately transferred into ice-cold fixative solution of 4% paraformaldehyde (Sigma-Aldrich, P6148) and 0.05% glutaraldehyde (Sigma-Aldrich 340855) solution for 3 hours. The fixative should be freshly prepared and kept ice cold during its use. During the dissection of organs, the adjacent muscles and fat should be removed completely as their presence may subvert the successful generation of whole organ overviews during imaging. The samples were then washed with PBS for 3 times at room temperature on a shaker. Each wash lasted for 5 minutes. From our experience, the fixed samples can be stored for up to 4 days at 4° C before moving forward with the bleaching or antigen retrieval and permeabilization. While placing tissues in fixative works well for several murine organs, the perfusion fixation with 4% PFA is recommended to facilitate instant fixation to preserve the life-like state of the tissues.

The fixative is hazardous; highly flammable and toxic and must be handled with appropriate PPE and other safety measures.

Bleaching

In larger heme rich organs bleaching was used to achieve maximum downstream organ clarity. Organs were immersed in a methanol gradient of 50%, 80% and 100% for 40 minutes each for dehydration. 100% methanol was changed twice, 20 minutes apart. These dehydration buffers should be ice-cold. Samples were then immersed in 5% (v/v) H_2O_2 in methanol for up to 3 hours (Sigma-Aldrich Cat No: H1009) for bleaching. Samples were then rehydrated with the reverse methanol concentrations. Following that, samples were washed three times with PBS for 20 minutes each. Dehydration for bleaching could also be achieved with Isopropanol that has a less toxic effect. However, methanol is better for removing pigmentation and more effective for delipidation. It also helps with membranes permeabilization and therefore antibody penetration.

Antigen Retrieval, Permeabilization and Collagenase Digestion

The fixed samples were subjected to antigen retrieval, and permeabilization with the ice-cold buffer containing 25% urea (VWR, Cat. No. 28876.367), 15% glycerol (VWR, cat. no. 24388.260) and 7% Triton X-100 (Sigma-Aldrich, cat. no. T8787) diluted with ddH_2O and incubated for 6 to12 hours at 4°C. Samples can then be directly processed to the next step of Collagenase based matrix digestion. Matrix digestion was performed with freshly prepared 0.2% Collagenase A (Merk, cat. no. 10103578001) prepared in PBS. Samples were incubated with Collagenase A solution for 30 minutes at 37°C on constant shaking. The Collagenase A solution should be freshly prepared.

The samples were then washed twice for 5 minutes with the wash buffer containing 2% FBS (Sigma-Aldrich, cat. no. F7524) in PBS.

Immunolabelling

For immunostaining, the organs were transferred to 5ml tubes and blocked in 10% donkey serum (Abcam, cat. no. ab7475), 10% DMSO with 0.5% Triton X-100 in PBS, at 37°C for 20 minutes. This blocking solution should be freshly prepared. Following blocking, the samples were incubated with the Alexa fluor conjugated antibodies or with the unconjugated primary antibodies. Primary antibody solution was prepared in 2% v/v donkey serum, 10% DMSO and 0.5% Triton-X-100 in PBS. The samples were incubated either overnight or for 14 to 16 hours at 37°C in a shaking water bath (Stuart, SBS40) rotating at 70 rpm with the primary antibodies (antibodies and dilution are listed in Table1). Following incubation, the samples were washed with 2% v/v donkey serum, and 0.5% Triton X 100 in PBS for 3 hours at 37°C in the shaking water bath rotating at 70 rpm. The wash buffer was changed every 15 minutes for the first hour and then every 30 minutes for the remaining 2 hours. For the unconjugated primary antibodies; after the washing steps, the samples were incubated with the Alexa fluor coupled secondary antibodies for 6 to 8 hours at 37°C in the shaking water bath rotating at 70 rpm. Secondary antibody solution was prepared in 2% v/v donkey serum, 10% DMSO and 0.5% Triton-X-100 in PBS. Following incubation, the samples were washed with 2% v/v donkey serum, and 0.5% Triton X 100 in PBS for 3 hours at 37°C in the shaking water bath rotating at 70 rpm.

Dehydration and tissue clearing

The immunostained samples were dehydrated in a gradient of isopropanol. Briefly, samples were immersed in a gradient of 30%, 50% and 80% (v/v) isopropanol for 30 minutes each under gentle rotation at room temperature. The organs were then immersed in 100% isopropanol for 1 hour with the 2 changes of isopropanol during this duration. The isopropanol was then completely removed, and the samples were rinsed twice with ethyl cinnamate (ECi) (Sigma-Aldrich, cat. no. 112372) for 5 minutes each. Samples were then cleared with 80% ECi and 20% poly(ethylene glycol) methyl ether methacrylate (PEGM) (Sigma, cat: 447943) under gentle rotation at room temperature for a minimum of 30 minutes.

Human samples

Formalin-fixed paraffin-embedded (FFPE) normal testis, ovary and thyroid gland blocks were ordered from AMS Biotechnology (Oxford, UK). Human specimens provided by AMS Biotechnology (Europe) Limited are legally procured under the laws and regulations of the country. All samples are collected from consented patients in the major research/clinical centres under the local EC/IRB-approved protocols. Samples from donors at ages 18-20 years and 70-80 years were selected to compare the young and aged groups, respectively. Histological study was performed to confirm that sample tissues were healthy and lack disease components. Further details on the healthy human tissue samples are provided (Table S3).

Imaging set-up, Image acquisition and Analysis

The cleared samples were imaged on the Miltenyi-LaVision Biotech UltraMicroscope II with the LaVision BioTech ImSpector software (MACs, Miltec bio). The microscope was equipped with a 2X objective lens for zoom body with a manual zoom of 0.63X–

14

6.3X. The objective was fitted with a Dipping Cap [5.7 mm] including correction Optics for Olympus MVPLAPO 2X. The microscope was fitted with the 405-100, 488-85, 561-100, 639-70 and 785-75 laser lines and the images captured with the Neo sCMOS camera (Andor). For image acquisition, cleared samples were manually attached with a drop of Superglue (No Nonsense, UK) to the sample holder adapter. Once the sample was firmly affixed to the sample holder, they were gently immersed in ECi in a quartz glass cuvette and excited with light sheets (30-90mm, dependent on organ size) of different wavelengths (488, 561, 640 and 785nm. The individual TIFF raw data images were converted by Imaris File converter (version 9.6.1, Bitplane) then analyzed by Imaris software (version 9.6.0, Bitplane).

Confocal immunofluorescent images of whole organs or regions of interesr were captured on a Zeiss Laser Scanning Microscope (LSM) 880 equipped with 7 laser lines (405, 453, 488, 514, 561, 594, and 633 nm), axio examiner (upright) stand and Colibri7 epifluorescence light source with LED illumination, the 10X Plan Apo 0.45 WD=2.0 M27 dry lens was used to image large regions using the tile scan function. Tiles were chosen based on organ size, and images were taken with a 10% overlap in order to stitch them together using Zen Black (version 3.1, Zeiss) software. Organs were imaged through the z-plane and reconstructed in Imaris in order to visualize the maximum intensity projection. In order to visualize the boundary of the organ, the autofluorescence from the 405 channel was converted into greyscale, and the 30% opaque image was manually overlayed with the corresponding TIFF file generated from Imaris. Imaris, Adobe Photoshop and Adobe illustrator software were used to generate, analyze and compile images.

3D surface rendering

To visualize components of the organ, 3D surface rendering was applied using the surface rendering tool in Imaris. First, the whole organ or region of interest (ROI) was defined and selected. Then, the smoothness of the resulting area was set up using the Smooth option. The threshold for background subtraction was manually annotated based on the individual image previewed.

Quantifications of imaging data

To quantify the vascular density of whole organs, quantifications were performed using the Imaris Surface Analysis XTensions tool. To obtain total tissue volume, the 3D crop tool was used and analyzed with the Volume statistics function of Imaris. A single channel lymphatic marker was reconstructed using the 3D rendering surface function, and the tissue volume of the vessels was measured by employing the Surface statistics function in Imaris. The density of the lymphatic vasculature was calculated, dividing the tissue volume of vessels in the numerator by the total tissue volume in the denominator.

Quantification of PROX1$^+$ cell number was done with Imaris software (version 9.2.1) based on single-cell resolution 3D images. Nuclei detection and membrane detection function in the Cell module of Imaris were used to automatically segment and analyze the numbers of PROX1$^+$ cells. Under the Cell Creation wizard of Imaris, PROX1 channel was selected as a source channel for membrane-based detection, and DAPI channel was selected for nuclei-based detection. Nuclei locations were used as seed points for an algorithm performing a cell membrane calculation, which was used to distinguish between the inner and outer boundaries of the cell. The number of PROX1$^+$ cells per tissue volume (mm^{-3}) was calculated by dividing the number of segmented cells in the numerator by the total tissue volume in the denominator.

Histology

Mice were sacrificed, and organs (liver, kidney, spleen and heart) were collected. One group of organs were fixed with 10% formalin in PBS. Another group of organs were fixed with 10% formation followed by the steps of SUMIC protocol (dehydration with gradient isopropanol and clearing with ECi). All samples were embedded in a paraffin block and sliced into 5 μm thick sections. Following H&E staining, the samples were imaged by bright-field microscopy (Olympus Co., Japan).

Quantitative PCR

For the analysis of *Prox1* expression levels from FPPE blocks of human endocrine tissues, 25 μm sections were generated from FPPE blocks. After deparaffinization, FFPE sections were immersed into xylene and then into 100% ethanol twice, followed by air drying for 15 min. Quantitative PCR (qPCR) was performed using TaqMan gene expression assays on ABI PRISM 7900HT Sequence Detection System. RNA extraction kit (QIAGEN, 73504) was used to perform RNA extraction based on the manufacturer's instructions. RNA samples were immediately processed for cDNA preparation using SuperScript IV First-Strand Synthesis System (Invitrogen, 18091200). The FAM-conjugated TaqMan probes were used along with TaqMan Gene Expression Master Mix (Applied Biosystems, 4369510). The relative expression level gene was normalized based on the *Actb*.

Statistical analysis

All statistical analyses were performed using GraphPad Prism software (version 9.1). All data are presented as mean± s.d. The significance of the difference in mean values

was determined using two-tailed Student's t-test. The statistical significance was declared when $P < 0.05$. ns: not significant; *: $P < 0.05$; **: $P < 0.01$; ****: $P < 0.001$; ****: $P < 0.0001$. No randomization or blinding was used, and no animals were excluded from analyses. Several independent experiments were performed to guarantee reproducibility of findings.

Acknowledgements

Author Contributions

L.B., J.C., J.D.A., A.C., S.K.R, and A.P.K. designed and organized the experiments. L.B., and J.C. performed most of the experiments. L.B., J.C., and A.P.K. analyzed data and interpreted results. J.N. and S.K.R. provided critical samples. M.L.D. contributed to the design of imaging setup, provided critical advice and commented on the

manuscript. J.C. prepared figures. J.C and A.P.K wrote the paper. L.B. wrote methods section. J.C., J.D.A., A.C. and A.P.K. edited the manuscript. A.P.K. conceived, devised and supervised the study and method development.

Author Information

The authors do not declare competing financial interests.

Conflicts of Interest

The authors have declared that no conflict of interest exists.

References

1. I. Salwig, B. Spitznagel, M. Wiesnet, T. Braun, Imaging lung regeneration by light sheet microscopy. *Histochemistry and Cell Biology*, (2020).
2. M. Belle *et al.*, Tridimensional Visualization and Analysis of Early Human Development. *Cell* **169**, 161-173.e112 (2017).
3. Y. Ding *et al.*, Multiscale light-sheet for rapid imaging of cardiopulmonary system. *JCI insight* **3**, e121396 (2018).
4. R. S. Udan, V. G. Piazza, C.-w. Hsu, A.-K. Hadjantonakis, M. E. Dickinson, Quantitative imaging of cell dynamics in mouse embryos using light-sheet microscopy. *Development* **141**, 4406-4414 (2014).
5. P. J. Keller, A. D. Schmidt, J. Wittbrodt, E. H. Stelzer, Reconstruction of zebrafish early embryonic development by scanned light sheet microscopy. *science* **322**, 1065-1069 (2008).
6. T. Takebe *et al.*, Massive and reproducible production of liver buds entirely from human pluripotent stem cells. *Cell reports* **21**, 2661-2670 (2017).
7. J. Huisken, J. Swoger, F. Del Bene, J. Wittbrodt, E. H. Stelzer, Optical sectioning deep inside live embryos by selective plane illumination microscopy. *Science* **305**, 1007-1009 (2004).
8. Y. Ding *et al.*, Light-sheet fluorescence imaging to localize cardiac lineage and protein distribution. *Scientific reports* **7**, 42209-42209 (2017).
9. C. Wolff *et al.*, Multi-view light-sheet imaging and tracking with the MaMuT software reveals the cell lineage of a direct developing arthropod limb. *Elife* **7**, e34410 (2018).
10. A. Singh *et al.*, Angiocrine signals regulate quiescence and therapy resistance in bone metastasis. *JCI Insight* **4**, (2019).

11. A. Klingberg *et al.*, Fully Automated Evaluation of Total Glomerular Number and Capillary Tuft Size in Nephritic Kidneys Using Lightsheet Microscopy. *J Am Soc Nephrol* **28**, 452-459 (2017).

12. A. P. Di Giovanna *et al.*, Whole-Brain Vasculature Reconstruction at the Single Capillary Level. *Scientific Reports* **8**, 12573 (2018).

13. B.-C. Chen *et al.*, Lattice light-sheet microscopy: imaging molecules to embryos at high spatiotemporal resolution. *Science* **346**, (2014).

14. E. A. Susaki, H. R. Ueda, Whole-body and Whole-Organ Clearing and Imaging Techniques with Single-Cell Resolution: Toward Organism-Level Systems Biology in Mammals. *Cell Chem Biol* **23**, 137-157 (2016).

15. S. Zhao *et al.*, Cellular and Molecular Probing of Intact Human Organs. *Cell* **180**, 796-812.e719 (2020).

16. P. H. Neckel, U. Mattheus, B. Hirt, L. Just, A. F. Mack, Large-scale tissue clearing (PACT): Technical evaluation and new perspectives in immunofluorescence, histology and ultrastructure. *Scientific Reports* **6**, 34331 (2016).

17. P. J. Keller, in *CLEO: 2015*. (San Jose, California, 2015), pp. JTu1D.2.

18. C. Prahst *et al.*, Mouse retinal cell behaviour in space and time using light sheet fluorescence microscopy. *Elife* **9**, (2020).

19. Z. Yang, P. Haslehurst, S. Scott, N. Emptage, K. Dholakia, A compact light-sheet microscope for the study of the mammalian central nervous system. *Scientific Reports* **6**, 26317 (2016).

20. M. I. Todorov *et al.*, Machine learning analysis of whole mouse brain vasculature. *Nat Methods* **17**, 442-449 (2020).

21. H. A. Messal *et al.*, Antigen retrieval and clearing for whole-organ immunofluorescence by FLASH. *Nature Protocols*, (2020).

22. Y. Sato *et al.*, Quick visualization of neurons in brain tissues using an optical clearing technique. *Anat Sci Int* **94**, 199-208 (2019).

23. R. M. Power, J. Huisken, A guide to light-sheet fluorescence microscopy for multiscale imaging. *Nat Methods* **14**, 360-373 (2017).

24. K. Matsumoto *et al.*, Advanced CUBIC tissue clearing for whole-organ cell profiling. *Nature Protocols* **14**, 3506-3537 (2019).

25. H. Hama *et al.*, ScaleS: an optical clearing palette for biological imaging. *Nat Neurosci* **18**, 1518-1529 (2015).

26. D. Jing *et al.*, Tissue clearing of both hard and soft tissue organs with the PEGASOS method. *Cell Res* **28**, 803-818 (2018).

27. F. Perbellini *et al.*, Free-of-Acrylamide SDS-based Tissue Clearing (FASTClear) for three dimensional visualization of myocardial tissue. *Sci Rep* **7**, 5188 (2017).

28. A. Azaripour *et al.*, A survey of clearing techniques for 3D imaging of tissues with special reference to connective tissue. *Prog Histochem Cytochem* **51**, 9-23 (2016).

29. M. K. Schwarz *et al.*, Fluorescent-protein stabilization and high-resolution imaging of cleared, intact mouse brains. *PLoS One* **10**, e0124650 (2015).

30. K. Chung *et al.*, Structural and molecular interrogation of intact biological systems. *Nature* **497**, 332-337 (2013).

31. N. Renier *et al.*, iDISCO: a simple, rapid method to immunolabel large tissue samples for volume imaging. *Cell* **159**, 896-910 (2014).

32. E. Murray *et al.*, Simple, Scalable Proteomic Imaging for High-Dimensional Profiling of Intact Systems. *Cell* **163**, 1500-1514 (2015).

33. A. Ertürk *et al.*, Three-dimensional imaging of solvent-cleared organs using 3DISCO. *Nature Protocols* **7**, 1983-1995 (2012).

34. H. U. Dodt *et al.*, Ultramicroscopy: three-dimensional visualization of neuronal networks in the whole mouse brain. *Nat Methods* **4**, 331-336 (2007).

35. H. Kolesová, M. Čapek, B. Radochová, J. Janáček, D. Sedmera, Comparison of different tissue clearing methods and 3D imaging techniques for visualization of GFP-expressing mouse embryos and embryonic hearts. *Histochem Cell Biol* **146**, 141-152 (2016).

36. A. Ludin *et al.*, Monocytes-macrophages that express α-smooth muscle actin preserve primitive hematopoietic cells in the bone marrow. *Nature immunology* **13**, 1072-1082 (2012).

37. K. Alitalo, The lymphatic vasculature in disease. *Nat Med* **17**, 1371-1380 (2011).

38. T. V. Petrova, G. Y. Koh, Biological functions of lymphatic vessels. *Science* **369**, (2020).

39. J. Chen *et al.*, Decreased blood vessel density and endothelial cell subset dynamics during ageing of the endocrine system. *The EMBO Journal* **n/a**, e105242 (2020).

40. Z. Xiao, Z. Dai, J. W. Locasale, Metabolic landscape of the tumor microenvironment at single cell resolution. *Nature Communications* **10**, 3763 (2019).

41. I. Sabdyusheva Litschauer *et al.*, 3D histopathology of human tumours by fast clearing and ultramicroscopy. *Scientific Reports* **10**, 17619 (2020).

42. B. Eismann *et al.*, Automated 3D light-sheet screening with high spatiotemporal resolution reveals mitotic phenotypes. *Journal of Cell Science* **133**, jcs245043 (2020).

43. N. Tanaka *et al.*, Whole-tissue biopsy phenotyping of three-dimensional tumours reveals patterns of cancer heterogeneity. *Nat Biomed Eng* **1**, 796-806 (2017).

44. E. Lee *et al.*, ACT-PRESTO: Rapid and consistent tissue clearing and labeling method for 3-dimensional (3D) imaging. *Scientific reports* **6**, 18631 (2016).

45. H. M. Lai *et al.*, Next generation histology methods for three-dimensional imaging of fresh and archival human brain tissues. *Nature Communications* **9**, 1066 (2018).

46. P. Uhlén, N. Tanaka, Improved Pathological Examination of Tumors with 3D Light-Sheet Microscopy. *Trends Cancer* **4**, 337-341 (2018).

47. A. K. Glaser *et al.*, Light-sheet microscopy for slide-free non-destructive pathology of large clinical specimens. *Nat Biomed Eng* **1**, 0084 (2017).

48. S. Nojima *et al.*, CUBIC pathology: three-dimensional imaging for pathological diagnosis. *Scientific Reports* **7**, 9269 (2017).

49. H. R. Ueda *et al.*, Tissue clearing and its applications in neuroscience. *Nat Rev Neurosci* **21**, 61-79 (2020).

50. E. A. Susaki *et al.*, Versatile whole-organ/body staining and imaging based on electrolyte-gel properties of biological tissues. *Nature Communications* **11**, 1982 (2020).

51. S. F. Merz *et al.*, Contemporaneous 3D characterization of acute and chronic myocardial I/R injury and response. *Nature Communications* **10**, 2312 (2019).

52. J. Huang *et al.*, A cationic near infrared fluorescent agent and ethyl-cinnamate tissue clearing protocol for vascular staining and imaging. *Sci Rep* **9**, 521 (2019).

53. W. Masselink *et al.*, Broad applicability of a streamlined ethyl cinnamate-based clearing procedure. *Development* **146**, dev166884 (2019).

54. M. Ema, S. Takahashi, J. Rossant, Deletion of the selection cassette, but not cis-acting elements, in targeted Flk1-lacZ allele reveals Flk1 expression in multipotent mesodermal progenitors. *Blood* **107**, 111-117 (2006).

55. L. Madisen *et al.*, A robust and high-throughput Cre reporting and characterization system for the whole mouse brain. *Nat Neurosci* **13**, 133-140 (2010).

56. A. P. Kusumbe, S. K. Ramasamy, R. H. Adams, Coupling of angiogenesis and osteogenesis by a specific vessel subtype in bone. *Nature* **507**, 323-328 (2014).

Legends to Figures

Fig. 1. Whole-organ 3D imaging using the simple ultrafast multicolor immunolabelling and clearing (SUMIC) method

Schematic illustration of a simple ultrafast multicolor immunolabelling and clearing (SUMIC) method for whole-organ imaging. After tissue harvesting and fixation (step 1), samples then go through bleaching (step 2, optional), antigen retrieval and permeabilization (step 3), collagenase digestion (step 4), immunostaining (step 5), dehydration (step 6) and clearing (step 7). Whole-organ images of cleared organs are acquired using a light-sheet or confocal microscope (step 8), and Z-stacks are subsequently 3D rendered and analyzed (step 9). After imaging, samples can also be used for histopathology (step 10, optional). The time shown for each step is the maximum time required to perform that step. The total time of the SUMIC is around 2.5 days. O/N, overnight.

Fig. 2. Light-sheet imaging of whole cleared organs using SUMIC

A) Photos (left) show mouse lung transparency before and after SUMIC. Representative images (middle) of whole cleared lung immuno-stained with Collagen IV and α-SMA acquired on a light sheet microscope. 3D image (right) of whole cleared lung immuno-stained with VEGFR2, α-SMA and Podocalyxin. **B)** Whole-organ imaging of cleared mouse heart stained with α-SMA (left), Collagen IV and α-SMA (middle) as well as SM22α (right). Inset shows high magnification of specific region. **C)** Light-sheet imaging of whole cleared mouse kidney staining as indicated. Inset shows high magnification of specific region. **D)** Photos (left) show mouse liver transparency before and after SUMIC. Representative 3D imaging (right) of whole

cleared liver immuno-stained with CD31 and α-SMA. **E)** Representative 3D imaging of whole cleared spleen immuno-stained with VEGFR2, CD31 and α-SMA.

Scale bars are 500 μm (A); Scale bars are 700 μm for whole-organ images and 200 μm for the high magnification insets (B); Scale bars are 500 μm (C-E).

Fig. 3. Light-sheet imaging of whole cleared endocrine glands using SUMIC

A) Photos (left) show mouse thymus transparency before and after SUMIC. Whole-organ 3D images (right) of cleared thymus stained with Endoglin and α-SMA acquired on a light sheet microscope. **B)** Photos (left) show mouse testis transparency before and after SUMIC. Representative 3D images (right) of whole cleared testis immuno-stained with the antibodies indicated in the panel. **C)** Whole-organ imaging of cleared mouse ovary stained with Decorin, α-SMA and VEGFR2 (left) as well as E-cadherin and α-SMA (right). **D)** 3D image of whole cleared prostate with α-SMA, CD44 and DAPI immunostaining. **E)** Light-sheet imaging of whole cleared adrenal gland immuno-stained with HSPG2 and α-SMA. **F)** Representative 3D imaging of whole cleared seminal vesicle stained with E-cadherin, α-SMA and VEGFR2.

Scale bars are 400 μm (A-C and E); Scale bars are 500 μm (D); Scale bars are 900 μm (F).

Fig. 4. 3D imaging of whole cleared endocrine glands and human tissues and detection of rare cells in whole organs using SUMIC

A) Representative 3D image of a cord of Dupuytren's disease immuno-stained with SOX9 and Endoglin (left) as well as α-SMA (right). Nuclei: DAPI. **B)** Representative 3D imaging of the cleared human liver with α-SMA immunostaining. **C)** Representative

3D images (left) of cleared ovary stained with CD102 from *Cdh5(PAC)-CreERT2; Rosa26-td-Tomato* mutant mice acquired on a confocal microscope. 3D images (right) of cleared ovary immuno-stained with BCAM from Flk-1 GFP reporter mice. Nuclei: DAPI. **D)** Representative 3D images (left) of cleared adrenal gland stained with CD102 from *Cdh5(PAC)-CreERT2; Rosa26-td-Tomato* mice. 3D images (right) of cleared adrenal gland from Flk-1 GFP reporter mice. Nuclei: DAPI. **E)** Whole-organ imaging of cleared mouse thymus stained with VEGFR2 and α-SMA acquired on a light sheet microscope. Inset shows high magnification of specific region. Arrowheads indicate α-SMA$^+$ stromal cells **F)** Representative 3D images (top) of cleared gut stained with Podoplanin (PDPN) and LYVE-1. Arrowheads (white) indicate Podoplanin$^+$ lymphatic endothelial cells. 3D images (bottom) of cleared testis stained with VEGFR2 and CD8a. Arrowheads (yellow) indicate CD8a$^+$ cells.

Scale bar is 400 μm (A-B); Scale bars are 100 μm (C); Scale bars are 150 μm for tile scan images and 50 μm for the high magnification insets (D). Scale bars are 400 μm for whole-organ image, 100 μm and 50 μm for insets (E); Scale bars are 50 μm (F).

Fig. 5. Age-associated lymphatic vessel declines in endocrine glands

A) Whole-organ imaging of cleared mouse ovary, testis and thyroid gland from young and aged mouse immuno-stained with LYVE-1. Asterisks indicate high magnification of specific areas in the different glands. Bar graphs show quantifications of lymphatic vessel density in young and aged ovary, testis and thyroid gland (*n=5*). **B)** 3D confocal images of young and aged ovary, testis and thyroid gland with Podoplanin and PROX1 immunostaining. Nuclei: DAPI. Bar graphs show quantifications of PROX1$^+$ cell number in young and aged ovary, testis and thyroid gland (*n=4*). **C)** qPCR analysis of

Prox1 expression (normalized to *Actb*) in the aged human ovary, testis and thyroid compared to young endocrine glands (*n=5*).

Data represents mean±s.d., p-value derived from two-tailed unpaired *t*-tests is given for all graphs. **: P <0.01; ***: P <0.001; ****; P <0.0001. Scale bars are 400 μm for whole-organ images and 50 μm for the high magnification insets (A); Scale bars are 50 μm (B).

Legends to Supplementary Figures

Fig. S1. Light-sheet imaging of whole cleared mouse organs and endocrine glands

A) Light-sheet imaging of whole cleared mouse lung with VEGFR2 and α-SMA immunostaining. **B)** Representative 3D images acquired on a light sheet microscope of whole cleared testis stained with the antibodies indicated in the panel. **C)** 3D image of whole cleared thymus stained with Emcn. **D)** Whole-organ imaging of cleared mouse liver stained with α-SMA and Emcn. **E)** Whole-organ imaging of cleared adrenal gland stained with Emcn.

Scale bars are 500 μm (A and D); Scale bars are 400 μm (B, C and E).

Fig. S2. SUMIC preserves tissue integrity, and the tissues can be used for histology

H&E staining of mouse kidney, liver, spleen and heart after fixation (up) and fixation followed by SUMIC processes (below).

Scale bars are 200 μm.

Fig. S3. Lymphatic vessel imaging in young versus aged murine organs

A-H) Whole-organ imaging of cleared mouse adrenal gland, kidney, liver, gut, muscle, lung, thymus and uterus with LYVE-1 immunostaining. Asterisks indicate high magnification of specific areas in the different organs.

Scale bars are 400 μm for whole-organ images and 50 μm for the high magnification insets (A-H).

Legends to Supplementary Tables

Table S1. List of primary antibodies thoroughly tested with SUMIC

Table S2. Troubleshooting table

Table S3. Details of healthy young and aged human endocrine gland tissue samples

Legends to Movies

Movie 1. SUMIC processed lung showing multicolor immunostaining for endothelial and perivascular cell markers.

Movie 2. SUMIC processed testis showing multicolor immunostaining for endothelial and perivascular cell markers.

Movie 3. SUMIC processed spleen showing multicolor immunostaining for endothelial and perivascular cell markers.

Movie 4. SUMIC processed thymus showing multicolor immunostaining for endothelial and perivascular cell markers.

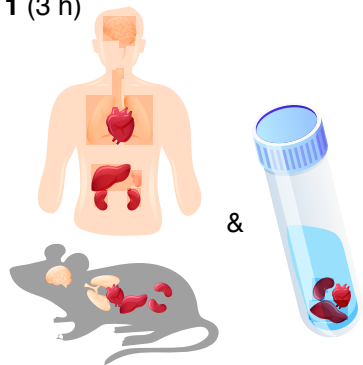**Movie 5**. SUMIC processed heart showing immunostaining for arteries.

Movie 6. SUMIC processed uterus showing immunostaining for a lymphatic marker.

Fig. 1

Fig. 2

A Endoglin/α-SMA
Thymus
→ SUMIC
Cleared
Cleared
Cleared

B α-SMA/CD31   Collagen IV/α-SMA/VEGFR2   α-SMA/Emcn/Decorin
Testis
→ SUMIC
Cleared
Cleared
Cleared

C Decorin/α-SMA/VEGFR2   E-Cadherin/α–SMA
Ovary

D DAPI/α-SMA/CD44
Prostate

E HSPG2/α-SMA
Adrenal Gland

F E-Cadherin/α-SMA/VEGFR2
Seminal Vesicle

Fig. 3

Fig. 4

Fig. 5

A VEGFR2/α-SMA
Lung

B CD102/α-SMA
Testis
α-SMA/Emcn
α-SMA/CD31

C Emcn
Thymus

D α-SMA/Emcn
Liver

E Emcn
Adrenal Gland

Fig. S1

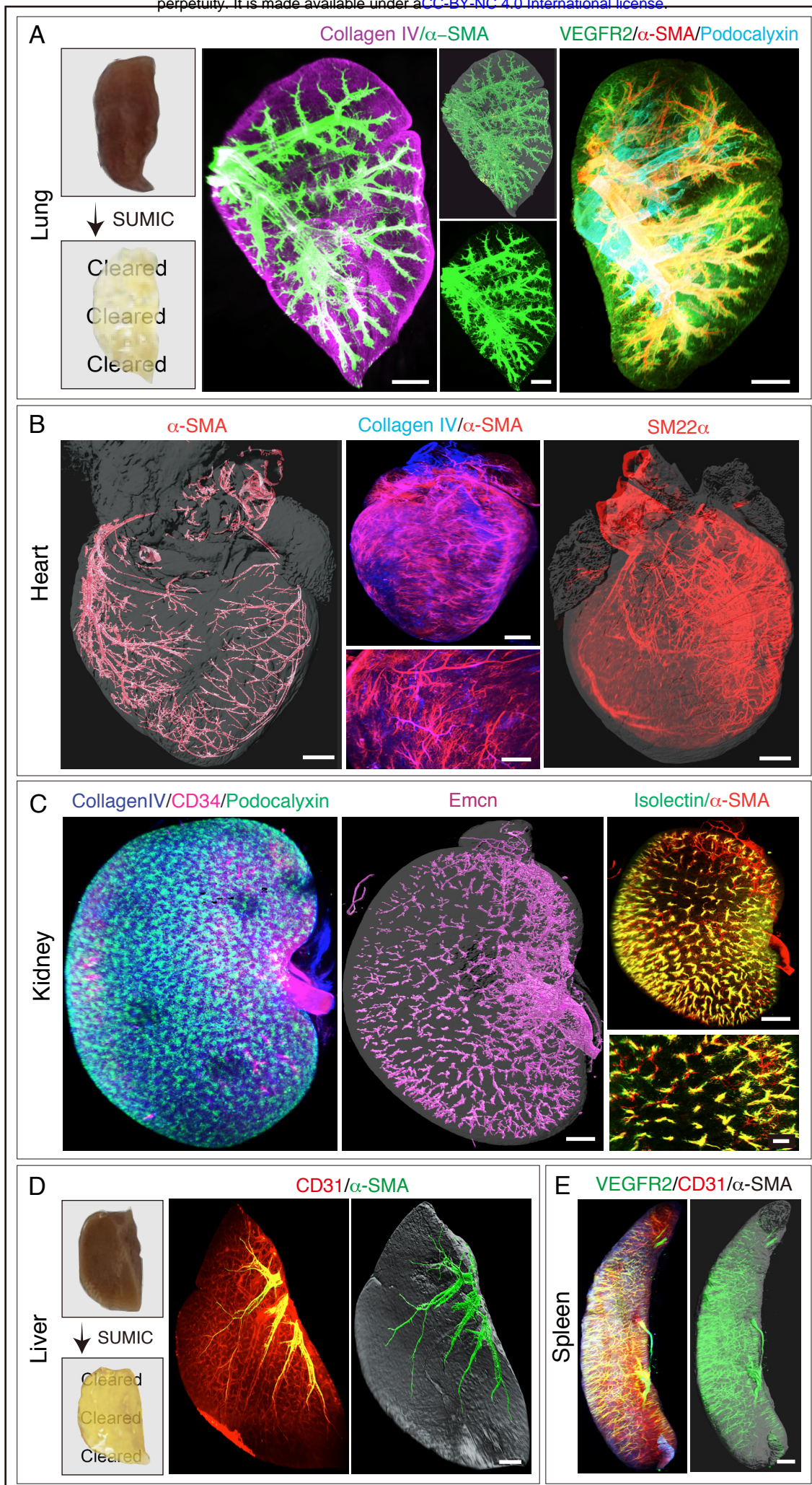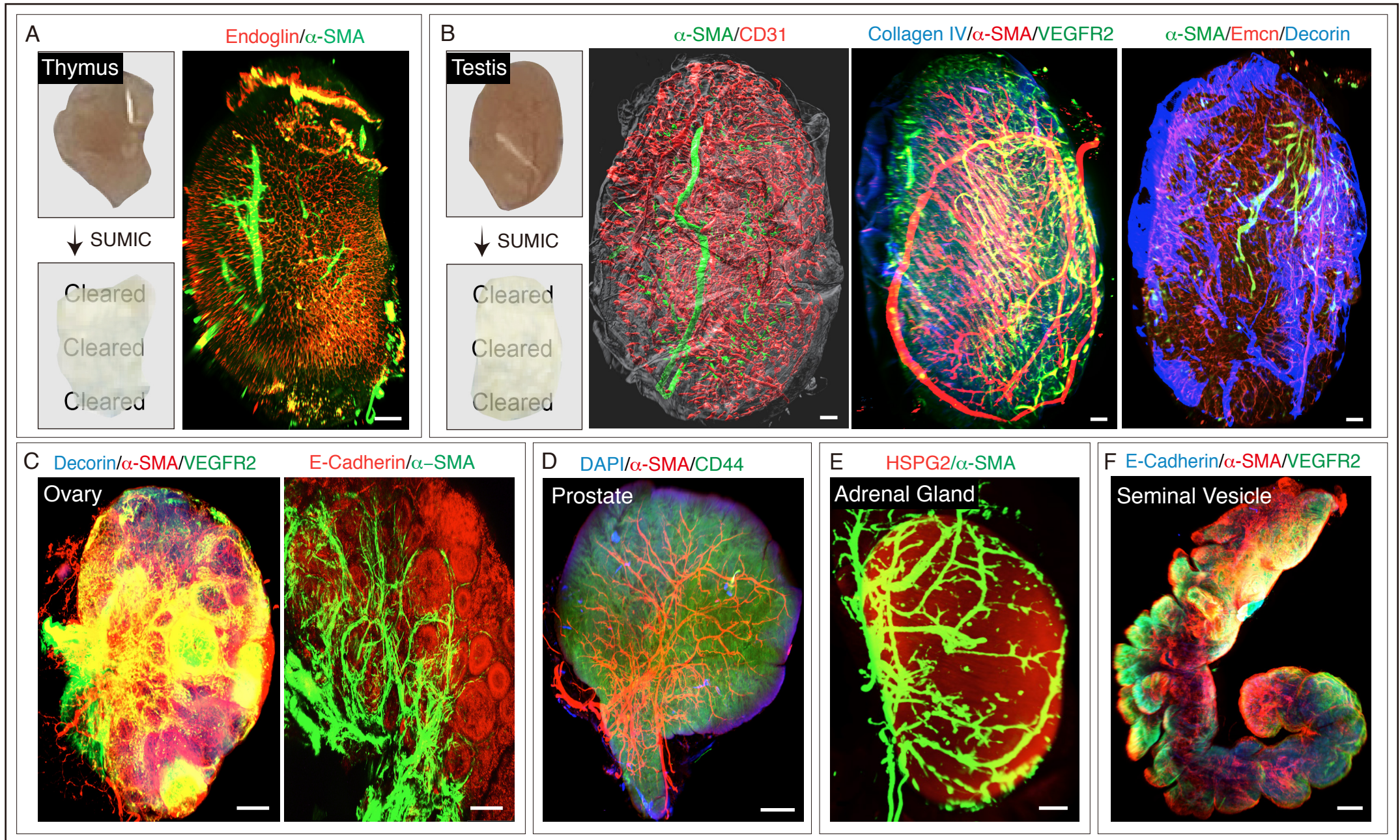|	Kidney	Liver	Spleen	Heart
After Fixation				
After Fixation+SUMIC				

Fig. S2

A Adrenal gland
B Kidney
C Liver
D Gut
E Muscle
F Lung
G Thymus
H Uterus

Young
Aged

LYVE-1
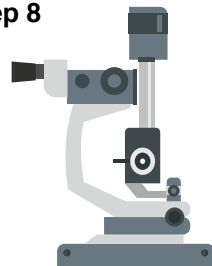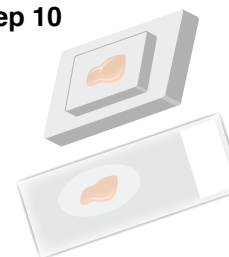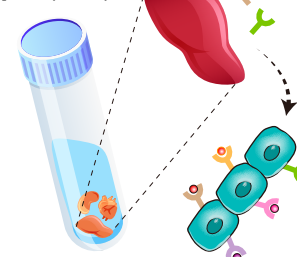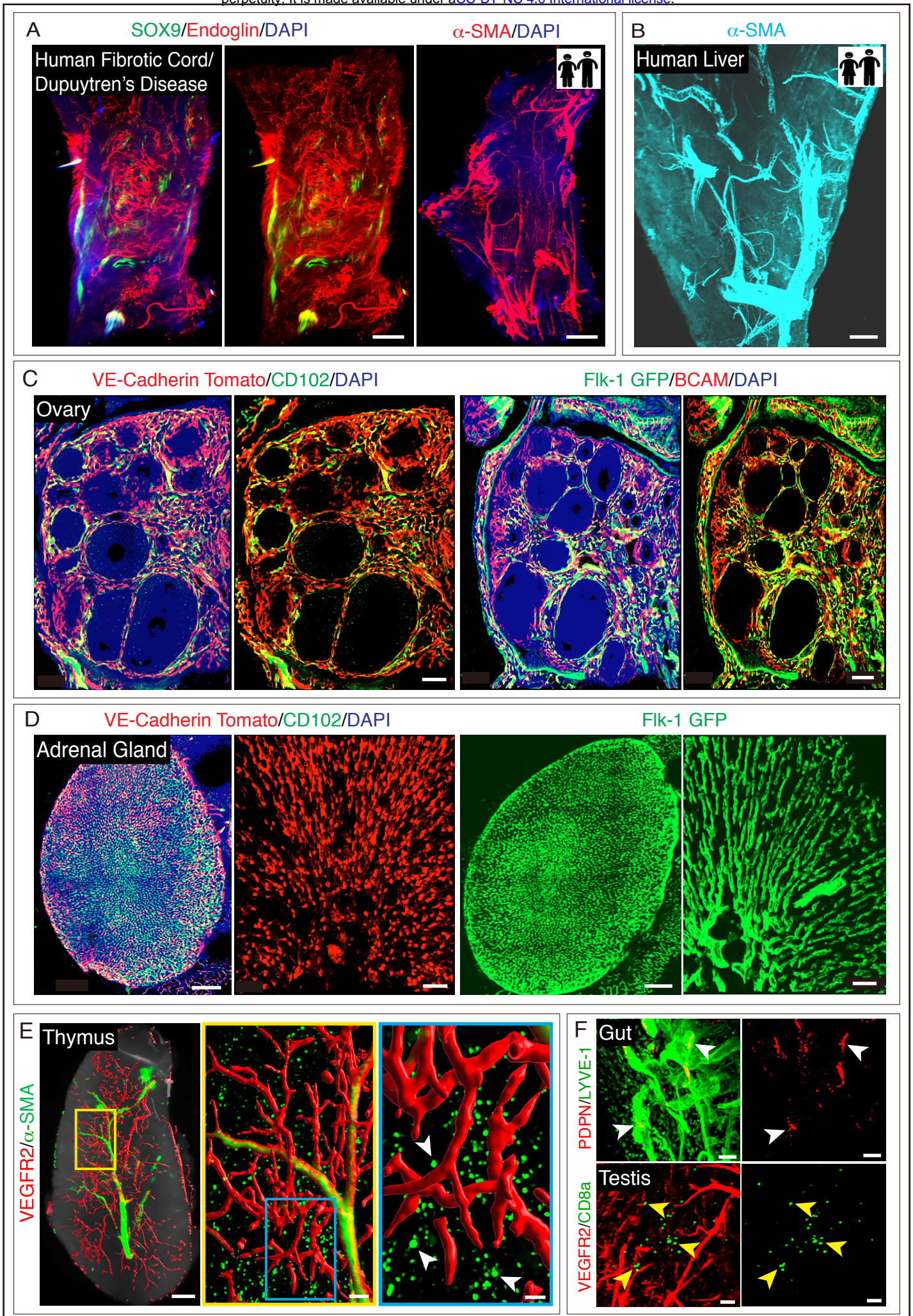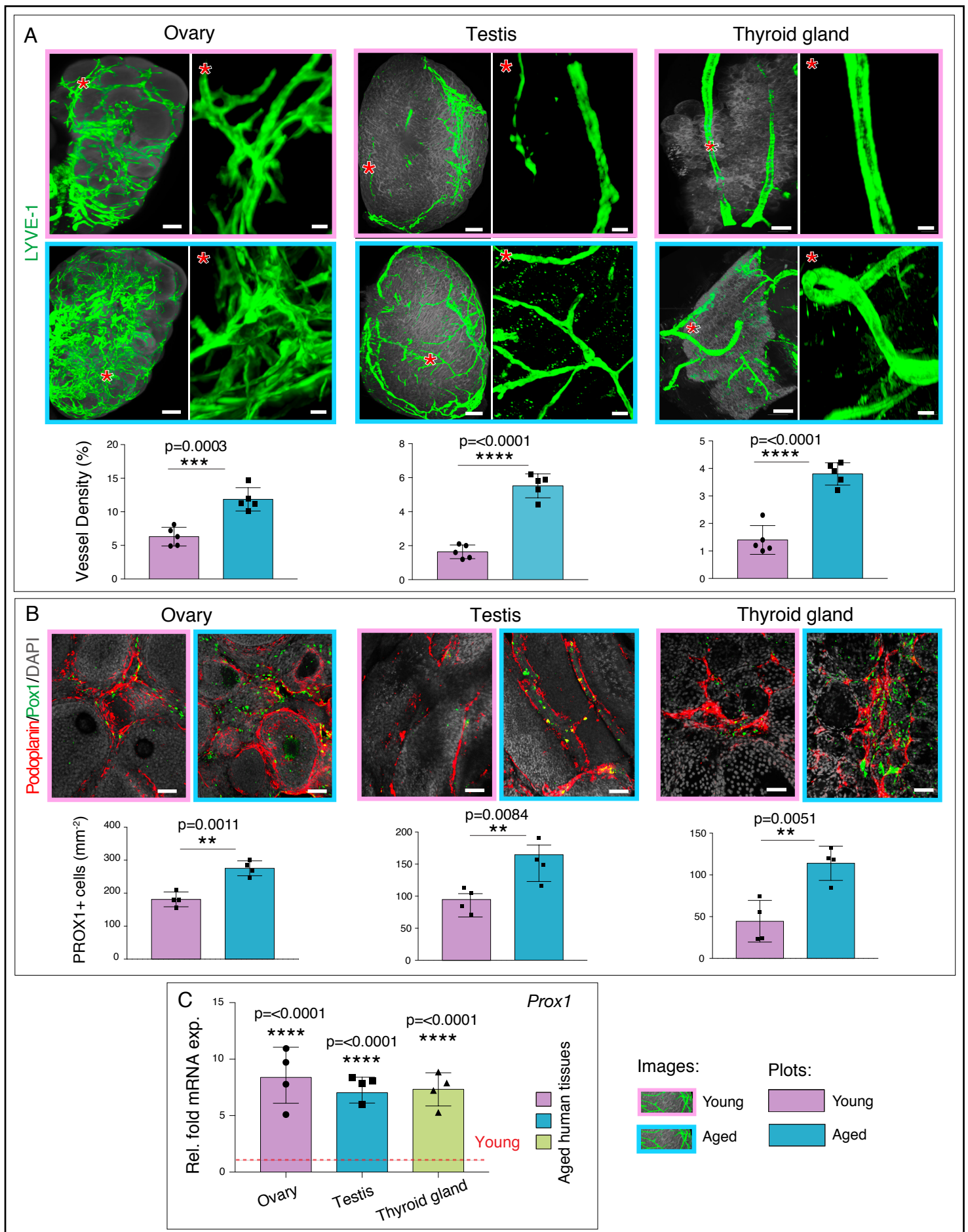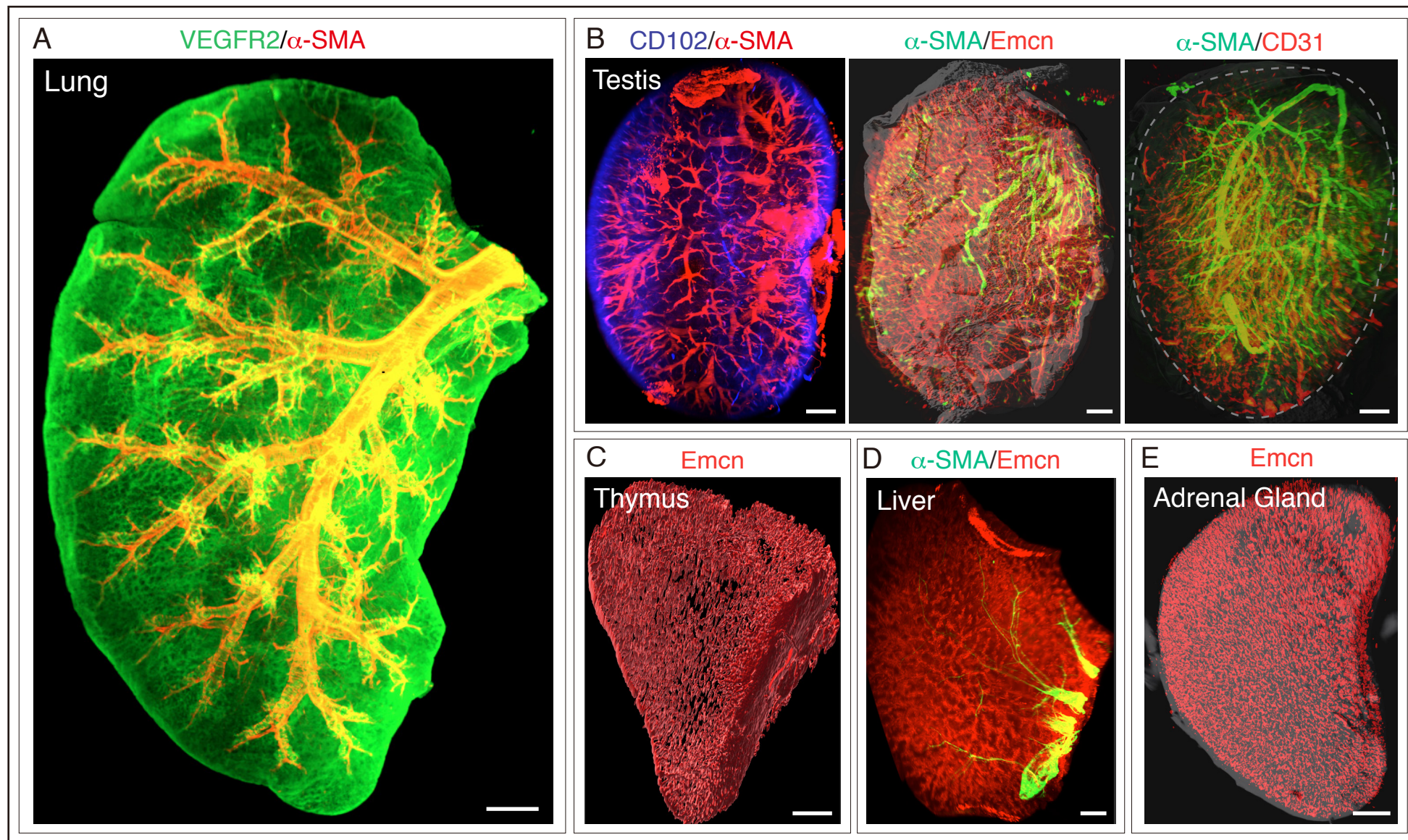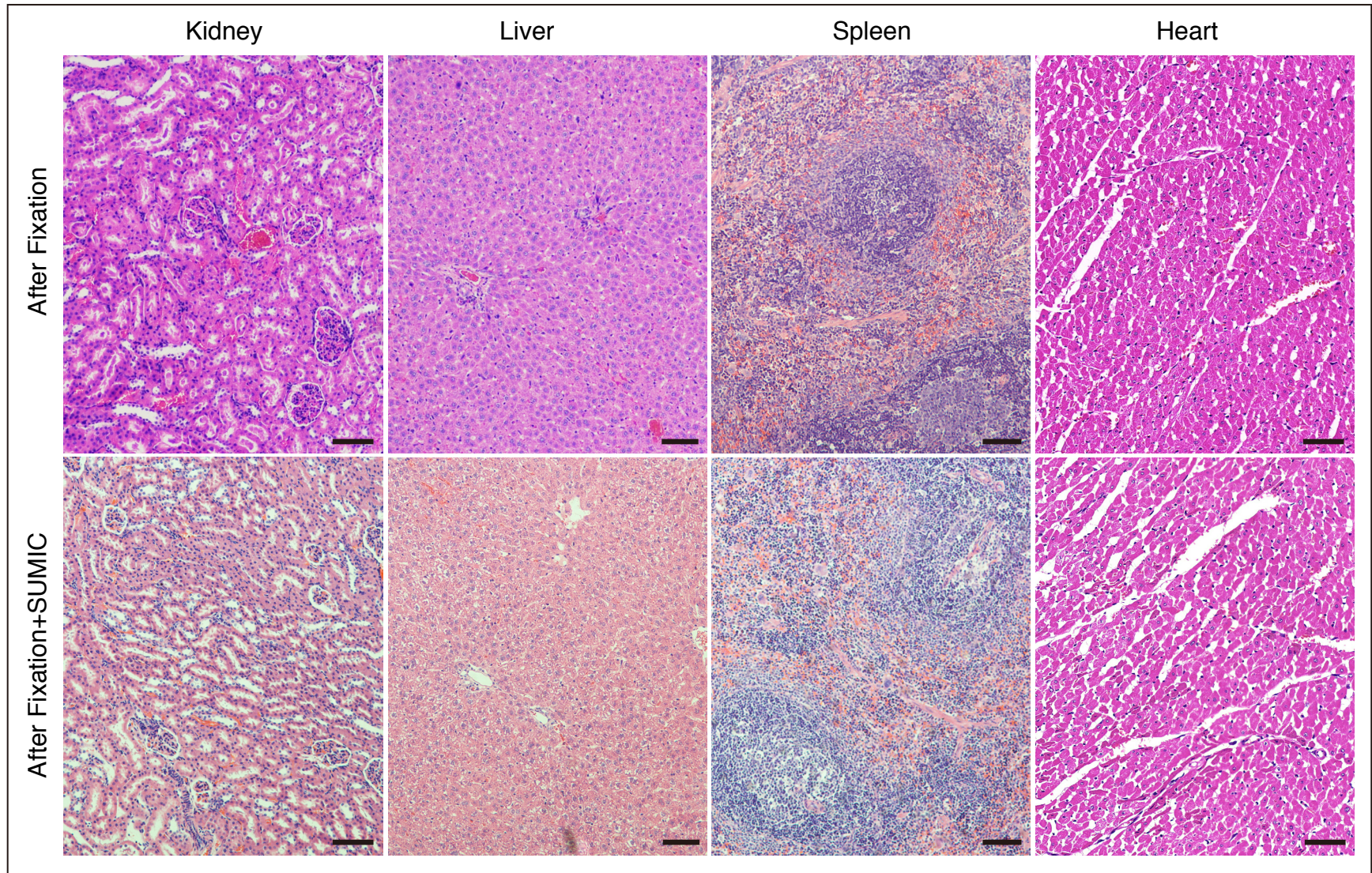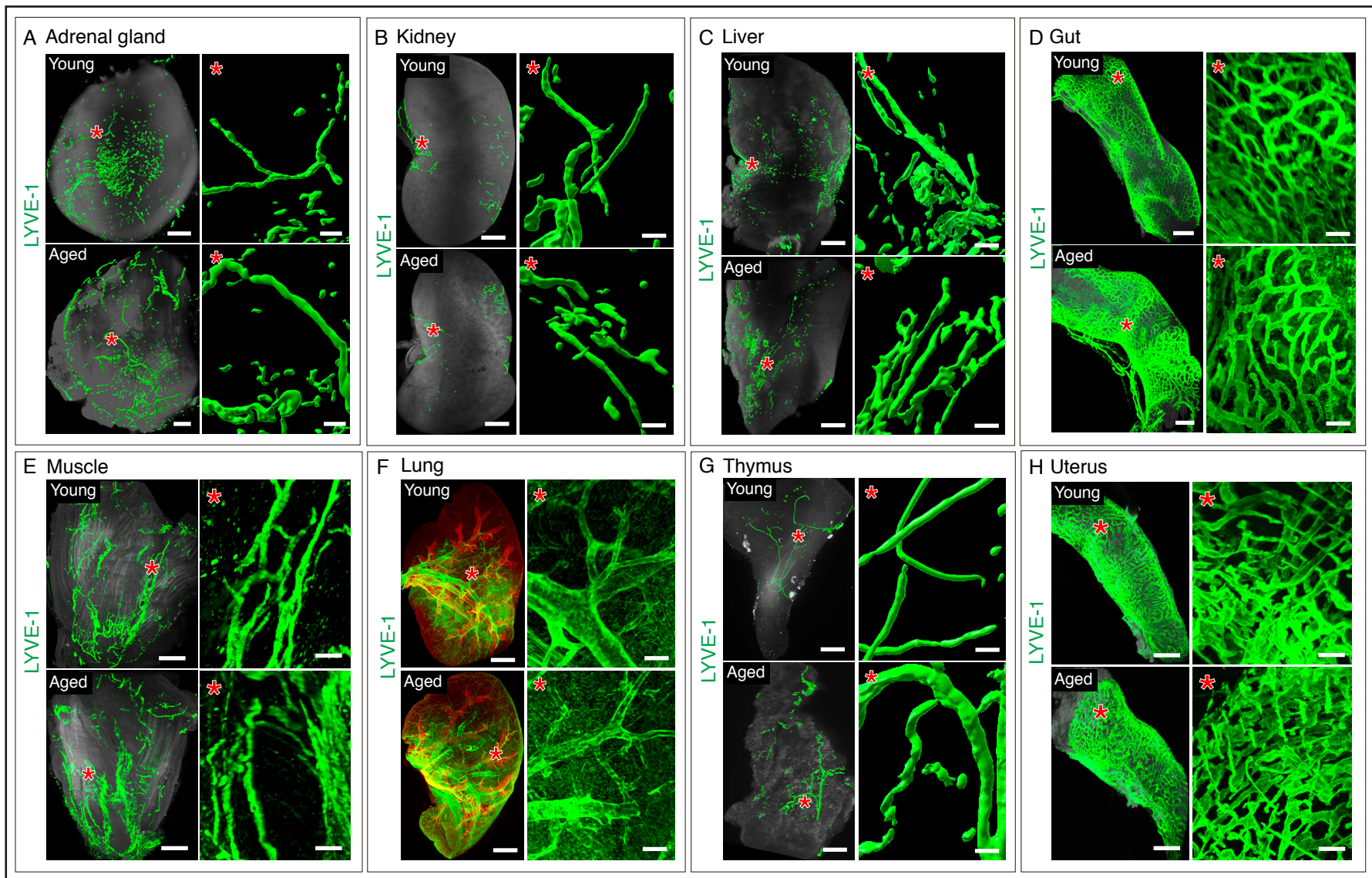
Fig. S3

Table S1. List of primary antibodies thoroughly tested with SUMIC

ANTIBODY	ALTERNATIVE NAME	CLONE	SPECIES	COMPANY	CAT NO.	CELL TYPE	DILUTION
α-SMA	ACTA1	IA4	Mouse	Sigma-Aldrich	C6198	Artery EC; Myoepithelial cell	1:500
Endomucin	Endomucin-2	V.7C7	Rat	Santa Cruz	sc-65495	EC	1:500
Collagen IV	COL4A3	Poly	Rabbit	Chemicon	AB756P	Matrix; EC	1:500
HSPG2	PLC	A7L6	Rat	Millipore	MAB1948P	Matrix	1:500
Isolectin	Isolectin B4	IB4	Biotinylated Griffonia	Vector Lab	B-1205	EC	1:500
FSP1	Calvasculin	Poly	Rabbit	Millipore	07-2274	Fibroblast	1:500
Pan Cadherin	Cadherin-1	EPR1792Y	Rabbit	Abcam	ab195203	EC	1:500
CD146	MCAM	EPR3208	Rabbit	Abcam	ab196448	EC	1:500
SM22α	Transgelin	Poly	Rabbit	Abcam	ab14106	Vascular SMC	1:500
CD144	VE-cadherin	Poly	Goat	R&D Systems	AF1002	EC	1:500
CD102	ICAM-2	3C4(mIC2/4)	Rat	BD Pharmingen	553326	EC	1:500
CD34	CD34 Molecule	RAM34	Rat	eBioscience	14-034-82	HSC; EC	1:500
CD31	PECAM1	MEC13.3	Rat	BD Biosciences	553370	EC	1:500
CD31	PECAM1	Poly	Goat	R&D Systems	FAB3628G	EC	1:500
Endoglin	CD105	Poly	Goat	B&D Systems	AF1320	EC	1:500
Endoglin	CD105	Poly	Goat	B&D Systems	AF1097	EC	1:500
Podocalyxin	PCLP1	Poly	Goat	B&D Systems	AF1556	EC	1:500
Decorin	DCN; PG40	Poly	Goat	B&D Systems	AF1060	MC	1:500
FABP4	A-FABP	Poly	Goat	B&D Systems	A1443	Adipocytes	1:500
CD44	PGP-1	IM7	Rat	BioLegend	103016	Multiple cell types	1:500
ESM-1	Endocan	Poly	Goat	R&D Systems	AF1999	EC/Tip cell	1:500
ESAM	LP4791 Protein	340236	Rat	R&D Systems	MAB28271	EC	1:500
Ki67	MKI67	Poly	Rabbit	Abcam	ab15580	Mitotic chromosome	1:500
Vinculin	VCL	EPR20407	Rabbit	Abcam	ab219649	Matrix	1:500
VCAM-1	CD106	Poly	Goat	R&D Systems	AF643	EC	1:500
E-Cadherin	CD324	Poly	Goat	R&D Systems	AF748	EC	1:500

Smoothelin	SMTN	EPR20044	Rabbit	Abcam	ab219652	SMC	1:500
Perilipin	PLIN1	D1D8	Rabbit	Cell signaling	9349	Adipocytes	1:500
NG2	CSPG4	Poly	Rabbit	Millipore	AB5320	Pericytes	1:500
P-selectin	SELP; CD62P	Poly	Goat	R&D Systems	AF737	EC	1:500
Laminin	LAMA1	Poly	Rabbit	Sigma-Aldrich	L9393	Matrix	1:500
ICAM-1	CD54	Poly	Goat	R&D Systems	AF796	EC	1:500
ICAM-1	CD54	EP1442Y	Rabbit	Abcam	ab53013	EC	1:500
TER-119	Ly-76	Mono	Rat	BioLegend	116202	Erythroid cells	1:500
LYVE-1	Extracellular link domain containing 1; XLKD1	Poly	Rabbit	Abcam	ab14917	Lymphatic EC; Macrophage	1:500
PROX1	Prospero-related homeobox 1	Poly	Rabbit	Abcam	ab101851	Lymphatic EC	1:500
Caveolin-1	CAV1; MSTP085	Poly	Rabbit	Cell signaling	3238	EC	1:500

EC: endothelial cell; HSC: hematopoietic stem cell; MC: mesenchymal cell; SMC: smooth muscle cell;

Table S2. Troubleshooting table

Problems	Possible reason	Solution
Weak antibody signal	Antibody concentration is inadequate to stain the whole organ	Optimize the antibody concentration
Noisy and non-transparent fluorescence signal	The dehydration may be limited. It also affects tissue clearing	Ensure the dehydration is enough to get transparent signal as per protocol
Antibody precipitations on the organ	Inadequate washing	Ensure adequate wash is carried out to overcome this issue
Appearance of nonspecific fluorescence signal	Precipitates and aggregates in the secondary antibodies	Avoid freeze-thaw cycles and the antibody should be spun down and mixed gently before use
High background along with antibody signal	Too much pigmentation and Hematoma on samples; Inadequate washing steps	Bleaching required to remove pigmentation and reduce hematoma signal; Wash more times
Fade antibody staining	Dehydration of chemicals	Optimised dehydration as suggested on the protocol
Tissue clearing and preservation of fluorescence signal	Slow tissue clearing and loss of fluorescence signal within few days	PEG increases the hydration capacity of the clearing medium and preserve longer fluorescence signal
Sometimes bubbles build up inside the whole organ	Hole in the organ and last hydration step	Fill the empty space in the organ with clearing solution by needle without damaging the tissues
Unstained or dark regions toward the centre to the organ/tissue	Collagenase digestion was either insufficient or unsuccessful	Collagenase solution should be freshly prepared; collagenase should be incubated at 37°C with constant shaking

Table S3. Details of healthy young and aged human endocrine gland tissue samples

Serial Number	Sample Name	Sample AMSBIO ID	Cataloge number	Age	Gender	Diagnosis	Ethnicity	Year of Procurement
1	Ovary	4765	AMS-33028	19	female	normal	Caucasian	09/11/2016
2	Ovary	5514	AMS-33028	18	female	normal	Caucasian	19/07/2015
3	Ovary	6379	AMS-33028	18	female	normal	Caucasian	03/12/2016
4	Ovary	7456	AMS-33028	19	female	normal	Caucasian	15/05/2017
5	Ovary	2108	AMS-33028	80	female	normal	Caucasian	30/07/2017
6	Ovary	1582	AMS-33028	79	female	normal	Caucasian	13/03/2017
7	Ovary	6715	AMS-33028	70	female	normal	Caucasian	12/01/2015
8	Ovary	4517	AMS-33028	72	female	normal	Caucasian	28/08/2016
9	Testis	149	AMS45022	18	male	normal	Caucasian	19/04/2016
10	Testis	152	AMS45022	19	male	normal	Caucasian	03/05/2017
11	Testis	154	AMS45022	18	male	normal	Caucasian	25/05/2017
12	Testis	156	AMS45022	20	male	normal	Caucasian	11/09/2018
13	Testis	29300	AMS45022	70	male	normal	Caucasian	22/09/2014
14	Testis	3509	AMS45022	71	male	normal	Caucasian	01/07/2014
15	Testis	3077	AMS45022	76	male	normal	Caucasian	27/08/2017
16	Testis	7267	AMS45022	75	male	normal	Caucasian	18/03/2017
17	Thyroid gland	0235	AMS-47028	18	female	normal	Caucasian	27/09/2015
18	Thyroid gland	3555	AMS-47028	19	female	normal	Caucasian	19/06/2015
19	Thyroid gland	5279	AMS-47028	19	female	normal	Caucasian	20/04/2015
20	Thyroid gland	6022	AMS-47028	20	female	normal	Caucasian	03/10/2016
21	Thyroid gland	4274	AMS-47028	71	female	normal	Caucasian	20/05/2016
22	Thyroid gland	3712	AMS-47028	73	male	normal	Caucasian	01/12/2015
23	Thyroid gland	2640	AMS-47028	70	female	normal	Caucasian	23/01/2016
24	Thyroid gland	4888	AMS-47028	72	female	normal	Caucasian	17/02/2017